AGU PUBLICATIONS

JGR

Journal of Geophysical Research: Solid Earth

RESEARCH ARTICLE
10.1002/2013JB010742

Key Points:
- CWI measurements combined to create continuous history of velocity change
- Velocities at MSH during this time period are dominated by seasonal effects
- Nisqually earthquake produced decrease in velocity; no intrusion signal observed

Correspondence to:
A. J. Hotovec-Ellis,
ahotovec@u.washington.edu

Citation:
Hotovec-Ellis, A. J., J. Gomberg, J. E. Vidale, and K. C. Creager (2014), A continuous record of intereruption velocity change at Mount St. Helens from coda wave interferometry, *J. Geophys. Res. Solid Earth*, *119*, doi:10.1002/2013JB010742.

Received 4 OCT 2013
Accepted 10 FEB 2014
Accepted article online 15 FEB 2014

A continuous record of intereruption velocity change at Mount St. Helens from coda wave interferometry

A. J. Hotovec-Ellis[1], J. Gomberg[2], J. E. Vidale[1], and K. C. Creager[1]

[1]Department of Earth and Space Sciences, University of Washington, Seattle, Washington, USA, [2]U.S. Geological Survey, University of Washington, Seattle, Washington, USA

Abstract In September 2004, Mount St. Helens volcano erupted after nearly 18 years of quiescence. However, it is unclear from the limited geophysical observations when or if the magma chamber replenished following the 1980–1986 eruptions in the years before the 2004–2008 extrusive eruption. We use coda wave interferometry with repeating earthquakes to measure small changes in the velocity structure of Mount St. Helens volcano that might indicate magmatic intrusion. By combining observations of relative velocity changes from many closely located earthquake sources, we solve for a continuous function of velocity changes with time. We find that seasonal effects dominate the relative velocity changes. Seismicity rates and repeating earthquake occurrence also vary seasonally; therefore, velocity changes and seismicity are likely modulated by snow loading, fluid saturation, and/or changes in groundwater level. We estimate hydrologic effects impart stress changes on the order of tens of kilopascals within the upper 4 km, resulting in annual velocity variations of 0.5 to 1%. The largest nonseasonal change is a decrease in velocity at the time of the deep $M_w = 6.8$ Nisqually earthquake. We find no systematic velocity changes during the most likely times of intrusions, consistent with a lack of observable surface deformation. We conclude that if replenishing intrusions occurred, they did not alter seismic velocities where this technique is sensitive due to either their small size or the finite compressibility of the magma chamber. We interpret the observed velocity changes and shallow seasonal seismicity as a response to small stress changes in a shallow, pressurized system.

1. Introduction

Mount St. Helens (MSH) is a dacite-andesite stratovolcano located in southwestern Washington State, famous for its massive explosive eruption in 1980. When it erupted again in late 2004, it did so with less than 2 weeks of warning, which took the form of vigorous shallow earthquake swarms [*Moran et al*., 2008; *Thelen et al*., 2008], GPS-measured deflation [*Dzurisin et al*., 2008; *Lisowski et al*., 2008], and visible deformation of the crater glacier [*Dzurisin et al*., 2008]. Petrologic studies of the eventually extruded magma found it was likely sourced near the top of the chamber (~5 km depth), largely degased, and similar to but chemically distinct from previous eruptions. This evidence can be interpreted as either due to tapping of a geochemically isolated region of the chamber or mixing with a fresh supply of low-gas dacite from depth [*Pallister et al*., 2008]. It is not clear whether this magma was introduced into the system before the end of the last eruption in 1986 or if the magma chamber was replenished during the intereruptive period. Distinguishing which of these two processes occurred is important for anticipating what MSH, and volcanoes like it, may do in the future.

There are limited geophysical data to constrain what occurred in the subsurface during the 18 years since the end of the previous dome-building eruption in late 1986 (Figure 1). A permanent GPS station installed at Johnston Ridge Observatory (JRO1, Figure 2) in 1997 and radar interferograms [*Poland and Lu*, 2008] recorded no measurable deformation attributable to the volcano between at least 1992 and September 2004. Earlier trilateration and campaign GPS further concur that although some measurable inflation occurred between 1982 and 1991, no measurable surface deformation occurred after [*Dzurisin et al*., 2008]. However, lack of geodetic evidence does not exclude the possibility that finite compressibility of the magma chamber could offset deformation due to an intrusion [*Dzurisin et al*., 2008; *Mastin et al*., 2008].

The most compelling evidence for magmatic intrusions during this time period is the occurrence of several deep (6–10 km depth) swarms of earthquakes [Moran, 1994]. The first burst of deeper seismicity occurred from 1987 to 1992. Focal mechanisms for these earthquakes were primarily strike slip, but with *P* axes

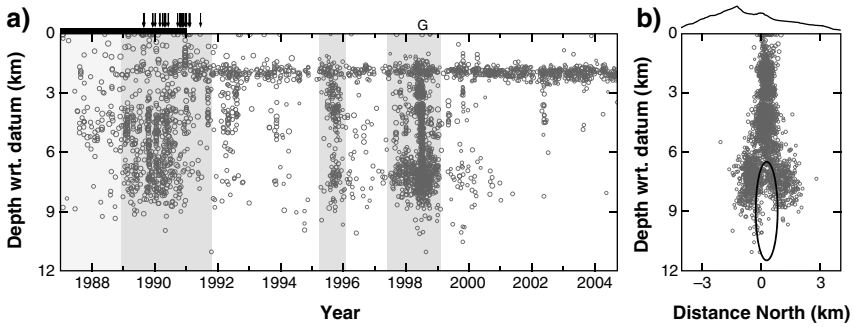

Figure 1. (a) Depth-time plot of well-located seismicity within 3 km of the dome (traveltime residual < .15 s, eight or more phases used, azimuthal gap ≤90°, and closest picked station within 5 km); coda wave interferometry was performed on all earthquakes in the catalog regardless of magnitude or location quality. Times of observed deformation from line length measurements (black bar), shallow explosions (arrows), and a gas emission (G) are also noted above the plot. Major swarms of deeper seismicity are highlighted in gray and have been interpreted in other studies as a response to magmatic intrusions. (b) Depth cross section through seismicity from south to north, centered on the dome. Depths are relative to a datum 1.1 km above sea level, which is the average elevation of stations in the seismic network near MSH; surface elevation of MSH is plotted above for reference. Hypocenters below 6 km surround an aseismic magma chamber, denoted by a black ellipse. The geometry of this chamber is the same used to model strain in Figure 11 [from *Lisowski*, 2006].

inconsistent with the regional trend. *Moran* [1994] modeled these focal mechanisms as an increase in pressure within a cylindrical magma chamber and interpreted the pressurization as being due to the sealing of the shallow conduit system, trapping exsolved magmatic gases. During this time, there was also a series of shallow gas explosions following rain and/or snow storms, interpreted as the explosive release of these trapped gases when water penetrated a low-permeability cap [*Mastin*, 1994]. Two more bursts of deep seismicity occurred from 1994 to 1995 and from 1997 to 1998. Several fixed-wing gas flights were flown between June and September 1998, when seismicity was at its peak. The first flight recorded gas emissions of 1900 t/d of CO_2, but the subsequent flights recorded only trace amounts or 0 t/d [*Gerlach et al.*, 2008]. Focal mechanisms of the deeper seismicity suggested another increase in pressure within the magma chamber. Hypocentral relocations of the seismicity by *Musumeci et al.* [2002] revealed that a large number of deeper earthquakes occur on at least two NE-SW striking, steeply dipping faults rather than being distributed around the chamber. They further suggested that the southeastern fault had slip consistent with magma being periodically injected into a truncated dike on the northwest side of the fault (i.e., right-lateral motion to the north of the chamber, left lateral to the south as the chamber expands).

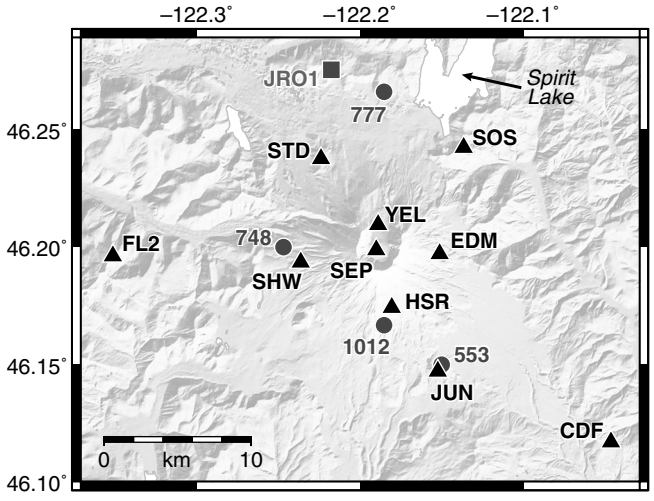

Figure 2. Map of GPS station JRO1 (gray square), SNOTEL stations (gray circles), and seismic network (black triangles) around Mount St. Helens. Seismic instruments are primarily L4 geophones, except HSR and CDF, which are S-13 geophones.

The state of the shallow subsurface is also relevant, as the overwhelming majority (>99%) of seismicity leading up to and during the 2004–2008 eruption occurred above 4 km depth [*Moran et al.*, 2008], and the eruption itself was potentially influenced by an abnormally wet late summer [*Scott et al.*, 2008]. The aforementioned shallow explosions from 1989 to 1991, which often also followed intense rainfall events, and shallow (<4 km depth), seasonally modulated [*Christiansen et al.*, 2005] seismicity suggest that the system above the magma chamber was also pressurized long before 2004 and sensitive to the influx of water and/or other small pressure perturbations of tens of

kilopascal. Focal mechanisms of these shallow earthquakes further suggest a complex stress regime best explained by localized increases in pore pressure from water and/or magmatic gases [*Lehto et al*., 2013].

In this study, we use coda wave interferometry (CWI) of repeating earthquakes at MSH to measure small changes in seismic wave speed in an attempt to better resolve the timing of magma injection and the pressurization of the magmatic system, as well as the evolution of the shallow (<4 km) subsurface, including the conduit. Small (<1%) changes in seismic velocity have been observed at a handful of other volcanoes prior to eruptions [*Ratdomopurbo and Poupinet*, 1995; *Wegler et al*., 2006; *Brenguier et al*., 2008a], during intrusive events [*Ueno et al*., 2012], in response to large earthquakes [*Battaglia et al*., 2012], and changes in groundwater hydrology [*Sens-Schönfelder and Wegler*, 2006]. These observations and laboratory results [*Grêt et al*., 2006] suggest that seismic velocity, in particular *S* wave velocity [*Snieder*, 2002], is sensitive to deformation and the opening/closing of cracks due to changes in stress, fluid saturation, and temperature.

2. Data

Figure 2 is a map of the local seismic network surrounding Mount St. Helens between January 1987 and September 2004. We use earthquakes that have epicenters and horizontal location uncertainty within 3 km of the volcano's summit (i.e., a 3.4 km distant earthquake with 0.5 km horizontal uncertainty would be included) and depths between 0 and 12 km relative to the datum of the local velocity model, approximately 1.1 km above sea level (Figure 1b). This area comprises the majority of located seismicity in the MSH vicinity related to the volcano. Seismicity beneath the volcano between 1 and 4 km depth is persistent across the nearly 18 year time span, whereas seismicity between 4 and 10 km mostly occurred in the three large swarms (Figure 1a). The earthquakes that we use in this study are cataloged and located by the Pacific Northwest Seismic Network (PNSN), using a network of Mark L4-C and Geotech S-13 single component, short-period, analog instruments operated by the PNSN and Cascades Volcano Observatory. During this time, the network configuration changed little, but instruments and VCO units were often replaced as part of normal station maintenance. Data from these stations were telemetered by radio to the PNSN in Seattle, WA. Until January 2002, only triggered data were saved, limiting the ability to study this time period with continuous methods such as ambient noise interferometry.

3. Application of Coda Wave Interferometry

Seismic velocities are dependent on the physical properties of the materials through which the seismic waves travel so that changes in these properties will produce a change in wave speed. Recent advances in theory and signal processing have allowed seismologists to observe small spatiotemporal changes in seismic velocities on the order of less than 0.1% by capitalizing on signals ordinarily discarded as noise. One technique for identifying velocity change is coda wave interferometry (CWI), wherein the codas of repeating earthquakes (also called repeaters, families, doublets, or multiplets) are compared. CWI operates under the theory that the seismic coda of two colocated earthquakes is a summation of multiply-scattered waves, and small changes in either the source or medium will affect how the scattered waves sum at the station and therefore alter the resulting waveform [e.g., *Snieder*, 2006]. The coda responds in distinct and predictable ways to different kinds of changes in the medium. For example, consider a widespread and uniform decrease in wave speed that occurs between the times of two colocated earthquakes with the same focal mechanism. Coda waves from the second earthquake will arrive with increasing delay as the waves travel a longer effective distance through the slower medium by multiple scattering [e.g., *Grêt et al*., 2006]. CWI measures an apparent velocity change, which is the average relative velocity change in the volume through which the coda waves propagate. It provides a lower bound on the maximum change, especially if the change is concentrated and compact. In the case of a localized change, coda waves are most sensitive to velocity perturbations in an ellipse with foci at the source and receiver locations but then increasingly less sensitive outside of that depending on the strength of scattering, frequency, and time lag [*Pacheco and Snieder*, 2005].

A change in seismic velocity is distinguishable from a change in source location, source mechanism, or scatterer location in that these other types of changes do not produce increasing lag with time for coda waves [*Snieder*, 2006]. For example, a change in location will alter coda wave paths, lengthening some and shortening others, but on average, the traveltimes will be the same, and the slope of lag with time will be

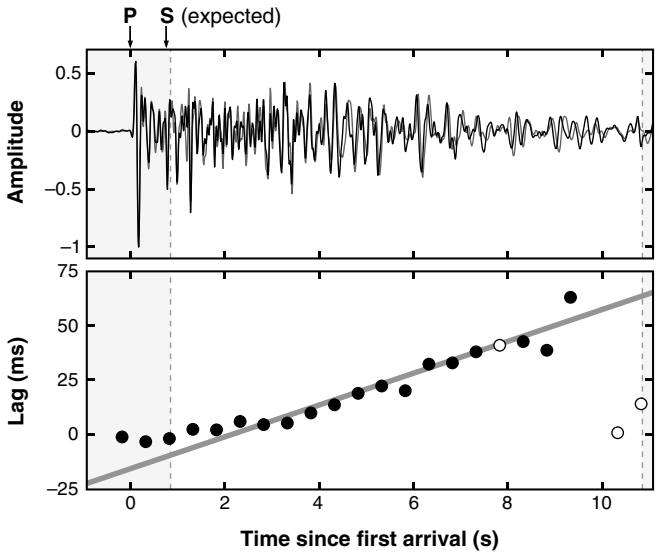

Figure 3. (top) Example of two earthquakes recorded at HSR that correlate well in the early waveform but decorrelate in the coda. *S* wave was not picked on either earthquake, so expected arrival time to station is estimated using the PNSN S3 velocity model. (bottom) Lag and similarity of black-to-gray waveform within nonoverlapping, 0.5 s windows, plotted as circles at the center of the time window and lag time to maximum correlation. Unshaded region between dotted lines denotes time window used to calculate slope of lags for velocity measurement; unfilled circles indicate windows where the CCC was below the 0.65 cutoff and were not used to determine slope. This slope corresponds to a relative decrease in velocity of 0.68%.

zero. Although on average the slope from these other changes will be zero, they still alter the waveform and introduce uncertainty in the calculation of relative velocity change difference between earthquake pairs.

CWI is ideally suited for use in volcanic settings because repeating earthquakes are commonplace at volcanoes [e.g., *Thelen et al*., 2011], sometimes even during noneruptive phases [*Saccorotti et al*., 2007; *Petersen*, 2007; *Carmona et al*., 2010; *Massin et al*., 2013], and the heterogeneity of the subsurface provides ample scattering. To find pairs of repeating earthquakes at MSH, we cross-correlate the entire 18 year catalog of 1–10 Hz band-passed waveforms on individual stations in a window 0.1 s before to 2.4 s after the analyst-picked *P* wave arrival, or the expected *P* wave arrival based on the locations of the earthquake and station in the absence of a pick. For each individual station, if the waveforms in this window correlate above a normalized cross-correlation coefficient (CCC) of 0.8, we consider the two earthquakes to be a possible repeating pair and realign the waveforms to the time of maximum correlation. Using these parameters, we find that earthquakes with at least one matching event account for approximately 40% of the catalog, with time gaps between some pairs of up to 10 years, but on average 1 year or less.

We then process each pair of repeating earthquakes using the doublet method of *Snieder et al*. [2002] to determine velocity changes. For each pair of repeating events we divide the two waveforms into nonoverlapping windows of 0.5 s length and calculate the CCC and lag for each window. We calculate the expected *S* wave arrival based on the earthquakes' location using the "S3" PNSN 1-D velocity model and $V_p/V_s = 1.78$ and only consider windows after that arrival as being part of the coda. If there are at least five windows in the coda that have CCC above 0.65, we fit a straight line to those lags (Figure 3). The slope of this line defines the relative velocity change, under the assumption that the change occurs uniformly throughout the entire contributing volume [*Snieder*, 2006]. This method is limited to velocity changes less than ~2 or 3%, as greater lags will reduce more windows below our 0.65 CCC cutoff. Clipping may also reduce the CCC, but only affects a small portion of our data set. We also attempt to account for slight differences in location of scatters, hypocenter, focal mechanism, and/or magnitude between the two earthquakes [e.g., *Kanu et al*., 2013] by only keeping pairs where the slope is well resolved and the standard deviation of the lags to the linear regression is less than 0.01 s. Although in theory the technique is precise to 0.01 or 0.02%, we estimate that our error for any given pair is closer to 0.1%. This is based on the standard deviation of velocity changes for pairs less than 10 days apart, where we expect the change on this timescale to be close to zero. This process is repeated for all possible earthquake pairs for each station out to 15 km distance from the summit of MSH.

Using the above procedure, we calculated relative velocity changes for thousands of event pairs separated by days to years. In reality, the relative velocity change is a function of both time and space, but at MSH we do not have the network density to fully resolve the spatial extent of our observed velocity changes. Therefore, in this paper we only solve at each station for the average velocity change with time within the volume through which the coda waves travel. Because different families of earthquakes occur near each other (within

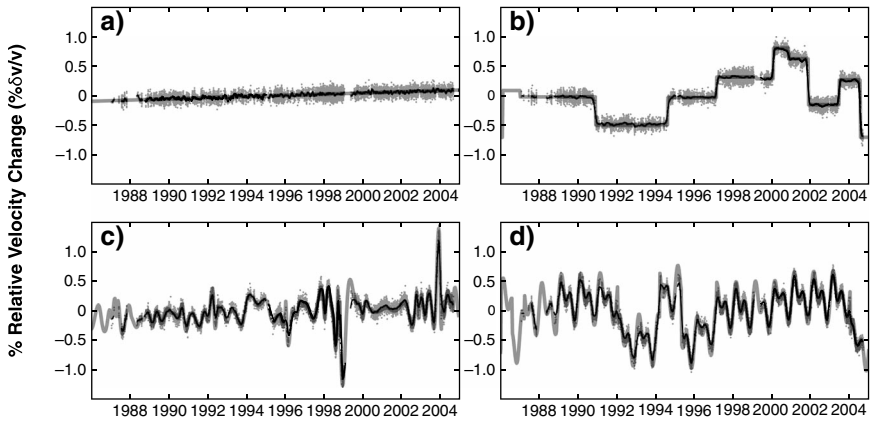

Figure 4. Tests of how well our inversion is able to recover a known function of velocity change (gray line) in the presence of Gaussian noise with standard deviation 0.1% d*v*/*v* and using the distribution of pairs at station HSR. The inverted solution (black line) has the best trade-off between misfit and smoothness. (a) A slope of 0.01%/yr with no other changes, (b) a series of small step functions, (c) a random spline function, and (d) the sum of two sinusoids (periods of 0.5 and 1 year) and a different series of step functions function than Figure 4b. Raw data points are plotted around the solution in gray.

a few kilometers or less) and sample much of the same volume, we combine observations from many nearby earthquakes into a single velocity-change chronology.

Relative velocity changes are often compared for pairs of doublets across an abrupt known geophysical event, such as a large earthquake [*Poupinet et al.*, 1984; *Nakamura et al.*, 2002; *Pandolfi et al.*, 2006; *Li et al.*, 2007; *Rubenstein et al.*, 2007; *Battaglia et al.*, 2012]. In this paper we instead assume that there is some continuous function of velocity with time and that each pair of earthquakes is sampling the difference between the velocities at those two times. We solve for the continuous function of velocity change that fits all the pairs of observed differential changes by a simple linear least squares inversion. The forward problem for any pair of earthquakes at times t_i and t_j is simply

$$d_{ij} = \gamma(t_j) - \gamma(t_i) \tag{1}$$

in which d_{ij} is the observed relative velocity change and $\gamma(t)$ is the continuous function of relative velocity change with time for which we intend to solve. We discretize the function $\gamma(t)$ evenly in time with a spacing of once every 10 days, i.e., the shortest amount of time we allow velocity to change over and linearly interpolate the function between each point. Therefore,

$$\gamma(t_i) = \gamma(t_k) + (\gamma(t_l) - \gamma(t_k))\frac{t_i - t_k}{t_l - t_k} \tag{2}$$

where k and l are the indices of γ on either side of t_i. Solving for γ is highly unstable because the problem is ill conditioned, so we are forced to regularize the inversion. We have chosen a combination of first- and second-order Tikhonov regularization (i.e., minimizing the first and second derivatives of the solution to favor a solution that varies slowly and smoothly) with equal weight and choose the solution with the best trade-off between roughness and misfit. Additionally, the mean is set to zero to further stabilize the inversion, as there is no constraint on the absolute velocity.

4. Inversion Results

Before we apply the inversion to real data, we can test how well it can resolve known functions of velocity change given the uneven sampling times from our real data. We have tested how well the inversion resolves no change, a linear increase, a series of step functions, and a sinusoidal function in the presence of Gaussian noise with standard deviation of 0.1%, our calculated error. Figure 4 shows what kinds of changes are resolvable when sampling a known continuous function at the times of earthquake pairs at station HSR, which has an average number of pairs but highly uneven sampling with time (i.e., repeating earthquakes occur more commonly during autumn than spring, discussed later). The primary discrepancies between the known input and the inversion result occur for times when the data are sparse, as expected. For this

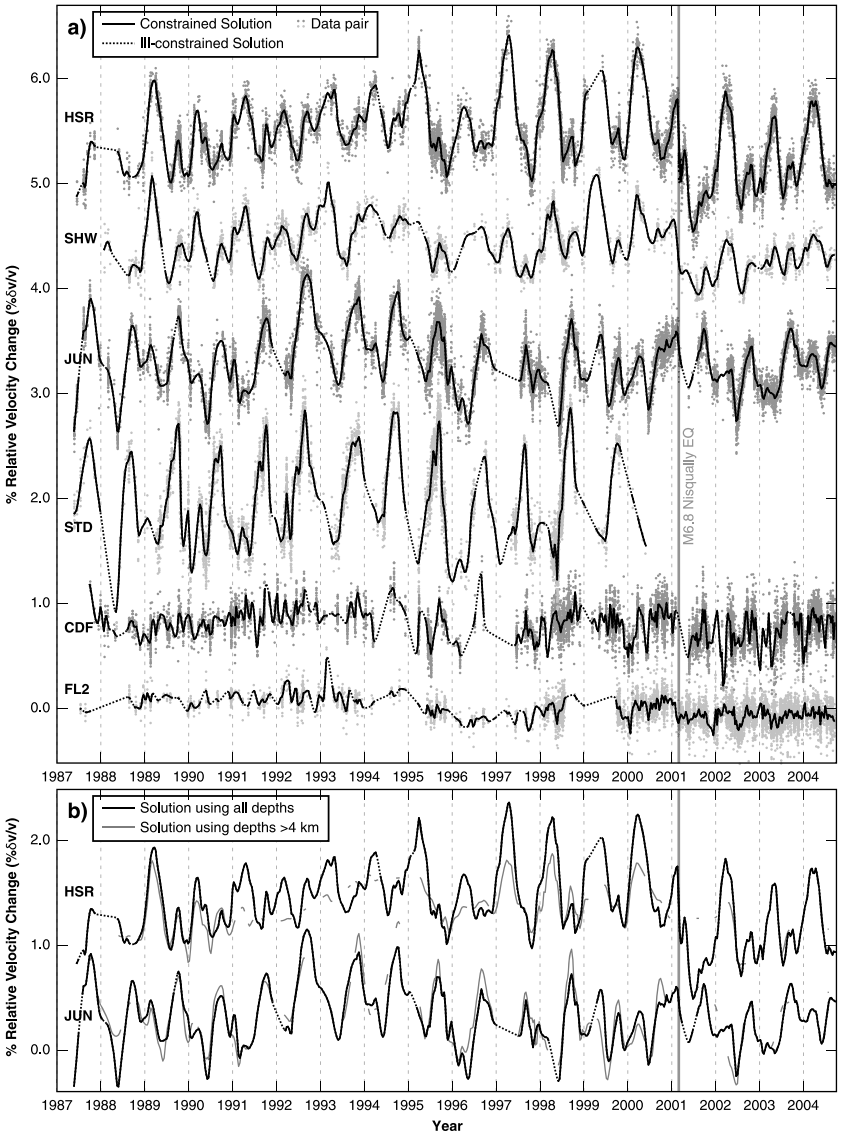

Figure 5. (a) Inversion results for shallow (<4 km; black line, dashed where solution ill constrained) earthquake pairs only. Gray dots represent the times and relative velocity changes of individual pairs of observations. For a single earthquake pair, one dot is plotted at the time of the first earthquake, the other at the time of the second, and their vertical separation is the observed velocity change between them. Pairs are plotted around the final solution such that if one dot is above the solution, the other is an equal distance below it. The dots serve to illustrate the temporal density of data, as well as uncertainty in the continuous solution. (b) Comparison of inversion solution using shallow (same as in Figure 5a) and deep (>4 km; gray line, not plotted where ill constrained) earthquake pairs separately for two representative stations. Solutions for deep and shallow source earthquakes are similar in timing and amplitude, indicating that the coda waves from both depth subsets are sampling similar, presumably shallow volumes. Vertical gray line in both plots corresponds to the date of *M*6.8 Nisqually earthquake. Results for stations SEP, YEL, EDM, and SOS are not plotted because there were an insufficient number of pairs to produce a stable inversion.

level of noise, the minimum resolvable step in velocity is ~0.2% and the minimum resolvable slope is ~0.01%/yr. Sinusoidal signals are well resolved where there are data and are not an artifact of uneven earthquake repetition.

For the first inversion involving real data, we incorporate only pairs with depths less than 4 km, which is where most seismicity occurs, and we can expect good temporal resolution. Figure 5 shows the result of the inversion for the six most densely sampled and reliable stations. Although there are some time periods

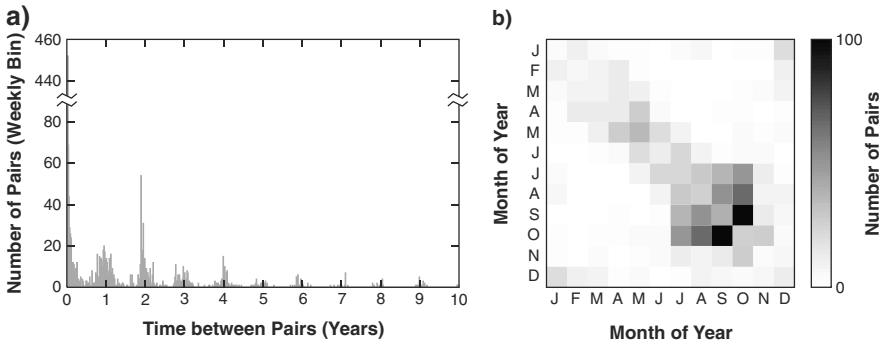

Figure 6. (a) Number of pairs of repeating earthquakes versus time between pairs in 1 week bins. Similar earthquakes repeat on yearly timescales and are not randomly distributed with time. (b) Matrix of number of pairs of earthquakes where one earthquake occurs in the month denoted by row, and the second occurs in the month by column. The matrix is symmetric, does not take into account which earthquake occurred first, and only includes pairs of earthquakes with time between earthquakes greater than 6 months. Although we have more pairs that occur each summer, pairs that occur in winter repeat primarily in winter. For both plots, only repeating earthquakes of *M*0+ and depths $<$4 km are included to reduce effects of biased sampling of smaller earthquakes during the summer and lack of sustained earthquakes at depth.

during which the solution is not well resolved, there is a strong annual cyclicity in the relative velocity change for most of the stations. The Fourier transform of the velocity change on the nearest four stations has a strong peak near 365 days, with a secondary peak around 183 days, indicating that the changes are seasonal. Since we are more interested in velocity changes due to changes within the volcano itself, we have also inverted for velocity change using a subset of earthquakes in the depth range 4 to 10 km, where we expected that changes from the magma chamber could be more visible due to a deeper source and sampling volume. Although the seismicity is more clustered in time, there are pairs of repeating earthquakes that span the gaps between swarms. Figure 5b also shows the remarkable similarity between relative velocity changes for the 1 to 4 km and 4 to 10 km depth ranges and demonstrates that seasonal velocity changes are stronger than any other signal from within the volcano for the entire depth range we consider. The similarity in amplitude of the annual velocity changes for both subsets further suggests that our coda waves are primarily composed of surface waves sampling the shallow subsurface, consistent with our 1–10 Hz band pass.

5. Seismicity Rate and Seasonal Repeaters

We observe a greater rate of repeating earthquakes during summer than winter when we include the entire catalog regardless of magnitude. *Christiansen et al.* [2005] found that *M*1.5+ earthquakes at MSH are statistically more common between July and October than during the rest of the year. There is still a possibility that this is in part an artifact of an incomplete catalog due to station health during the winter. *Christiansen et al.* [2005] attribute the increased seismicity to reduced normal stress from snow unloading and/or increased pore pressure of between 8 and 64 kPa from a rise in groundwater level by pore pressure diffusion.

Another observation is that the time between pairs of earthquakes is not randomly distributed but has annual cyclicity and further suggests that seismicity and stress changes in the shallow subsurface are seasonal in nature. Figure 6 illustrates that although most pairs of earthquakes have less than 6 months of time between them, there are a significant number of pairs that recur on a nearly yearly basis. Pairs that occur only in summer dominate the seasonal recurrence of repeating earthquakes, but other seasons show a similar preference. If the shallow, heterogeneous stress field is changing throughout the year from hydrologic changes, then the different families of earthquakes could be responses to those changes. That is, earthquakes that happen in the winter might have different orientations than the earthquakes during the summer, and although they may be located close to one another, they don't have similar waveforms.

6. Interpretation

6.1. Seasonal Variation as Climatological Loading

Comparing the relative velocity change as a function of time within each year reveals that the largest changes in velocity do not occur with the same pattern on every station (Figure 7). Stations on the volcano (HSR and

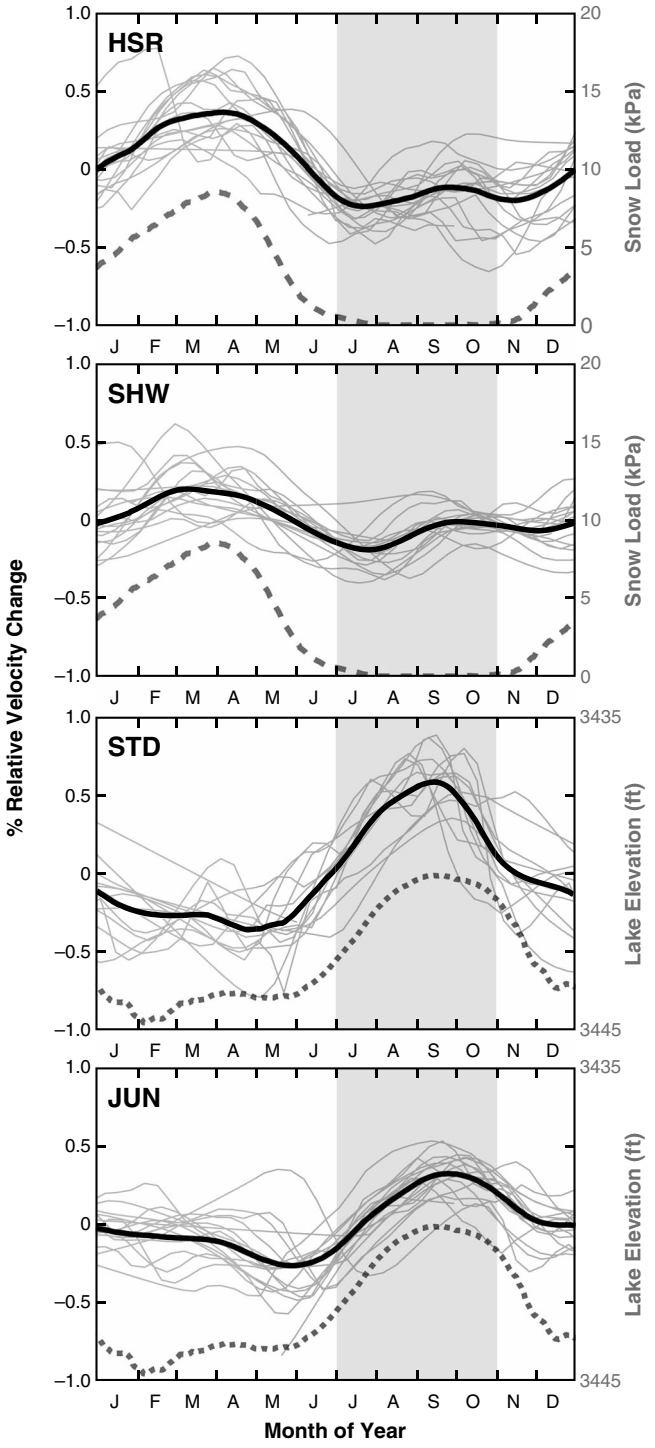

Figure 7. Velocity as a function of month of year, demeaned raw solutions in light gray and average in thicker black. Dashed line corresponds to average yearly snow load at SNOTEL station 748 in Sheep Canyon. Dotted line corresponds to average lake elevation at Spirit Lake, plotted with an inverted *y* axis to better illustrate the anticorrelation. Shaded area denotes months of the year with increased shallow seismicity from *Christiansen et al*. [2005].

SHW) have the highest relative velocity changes in the spring months (March through May), while stations off the volcano (STD and JUN) have highest changes in the late summer and early autumn (August through October). Although less obvious, the timing of the secondary peak for stations on the volcano aligns with the primary peak for stations off the volcano, and vice versa. To test how well the differences between stations are actually resolved by the inversion, we can compare the reduced chi-square misfit $\left(\chi^2_{\text{red}}\right)$ for the data at each station with various velocity change models, $\gamma(t)$. For example, a χ^2_{red} value calculated for the data from HSR and model from JUN of close to 1 would indicate that the model fits the data within the measurement uncertainties and accounts for the number of degrees of freedom. Table 1 summarizes the values of χ^2_{red} for data from the six best stations and models with no velocity change, the best model for that station, HSR's best model, JUN's best model, and a model using data from all stations in the same inversion. Perhaps unsurprisingly, using the model of JUN with the data from HSR (and vice versa) results in a significant increase in the misfit, even more than the assumption of zero change. We conclude that the models of velocity change are unique and resolvable from each other.

Given that the difference in amplitudes between stations is resolvable, the differences most likely represent different processes to which stations have varying sensitivity with an ~6 month offset and recurrence interval of 1 year. The high relative velocity in March corresponds to the peak annual snowpack, which we have verified using four SNOTEL stations in the Mount St. Helens vicinity (Figure 2) and would act to increase the velocity by closing cracks due to increased surface loading. The general shape of the snowpack curve (Figure 7) corresponds to the velocities at stations nearest the volcano (HSR

Table 1. Comparison of χ^2_{red} Misfit of Data to Different Models

	Zero Change	Best Fit	HSR Model	JUN Model	Hybrid Model
HSR	6.26	2.25	2.25	8.00	4.78
SHW	5.15	1.84	3.73	5.99	3.53
STD	4.09	1.86	6.26	3.19	2.93
JUN	5.64	1.86	8.11	1.86	2.73
CDF	2.16	1.51	6.81	3.84	2.08
FL2	1.90	1.51	11.07	5.65	2.39

and SHW) with nearly zero lag. Also, HSR and SHW would receive more snow than JUN and STD due to their elevation, and the relatively slower velocities in spring 1996 that occurred during a year with lower snowpack further suggest a causal relationship (Figure 8a).

The later peak in relative velocity in September corresponds to times when earthquakes occur more frequently. It seems to us an unlikely coincidence that increased velocity and earthquakes occur during the same time of year. One possibility is that an increase in the height of the groundwater table increases pore pressures and reduces local effective normal forces, resulting in more frequent earthquakes. In addition, an increase in the height of the groundwater table could increase velocities by closing cracks due to the weight of the water, similar to snow pack, or through poroelastic effects. Although no direct measures of the groundwater table are available in the area, lake elevation data from Spirit Lake may be used as a proxy and constraint on groundwater models. Simple hydrologic modeling by *Christiansen et al.* [2005] indicates that the groundwater level change is on the order of 1 to 9 m. The timing of the maximum highs in modeled groundwater levels qualitatively coincides with the onset of increased seismicity rate and relative velocity increases. A complication of this interpretation is that the depth of the water table is unknown but could potentially be several kilometers deep [*Hurwitz et al.*, 2003] or only a few tens of meters deep if there is a perched aquifer [*Bedrosian et al.*, 2008].

Lake level data serve as a proxy for groundwater changes. When lake elevation is compared to velocity (Figures 7 and 8b), we find that the two are anticorrelated. The September peak in velocity increases at STD, and JUN corresponds to lower lake elevations, suggesting that shallow water loading is likely not affecting

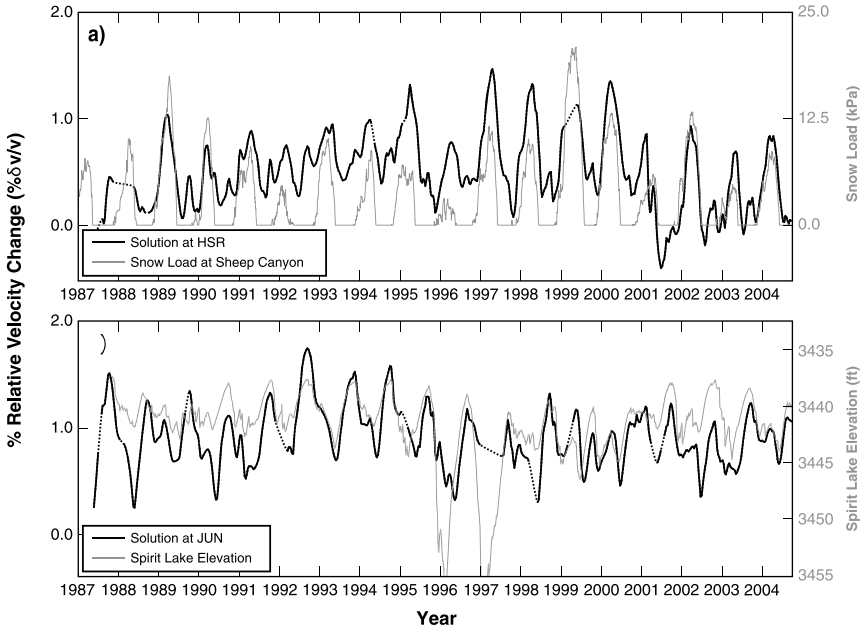

Figure 8. (a) Comparison of full velocity record at HSR with snow load. Note that lower velocities in 1996 correspond to a winter with lower snow loading. (b) Comparison of full velocity record at JUN with elevation of Spirit Lake, which we use as a proxy for shallow fluid saturation. Lake elevation is plotted with an inverted *y* axis to emphasize anticorrelation of saturation with velocity.

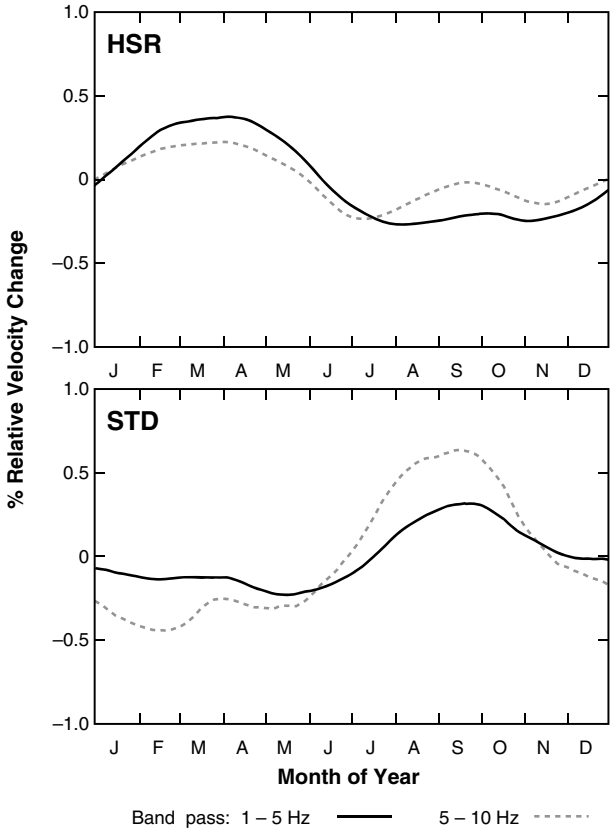

Figure 9. Velocity as a function of month of year in two different frequency bands (1–5 Hz and 5–10 Hz) at stations HSR and STD. The difference between the 1–5 and 5–10 Hz bands suggests that the velocity changes in spring are deeper than the changes in autumn, due to the frequency-dependent depth sampling of surface waves in the coda.

the velocity. We propose instead that at the lower elevations of STD and JUN, velocities reflect fluid saturation in the shallow subsurface, such that decreased water saturation (indicated by low lake level) increases the velocity, and vice versa [e.g., *Grêt et al*., 2006]. At higher elevations, velocity changes are smaller during this time of year, so fluid saturation may not change much seasonally. We note that lake level was abnormally high in early 1996 and 1997 compared with other years, but this does not correspond to extraordinary decreases in the velocity change record. We presume during most years that complete saturation was achieved, and during those 2 years, lake level increased beyond the level corresponding to full saturation and had no extra effect. Changes in saturation are likely very shallow (on the order of perhaps a few meters) and should not affect seismicity at depth. Therefore, the simplest explanation of correlation between seismicity and velocity is that seismicity is more related to snow unloading and anticorrelated with the higher velocities in winter.

Let us also briefly consider other possible candidates for seasonal changes in velocity. Thermoelastic strain (i.e., deformation related to spatiotemporal variations of temperature) could also produce seasonal velocity changes through seasonal changes in temperature [*Ben-Zion and Leary*, 1986; *Meier et al*., 2010] but does not readily explain the generation of seasonal earthquakes or the discrepancy in sensitivity between stations. Daily to weekly variations in barometric pressure of a few kilopascals have been shown to alter velocities in wells [e.g., *Silver et al*., 2007], and barometric pressure also varies seasonally. Barometric pressure is not measured at SNOTEL stations near Mount St. Helens, and the nearest comparable station (approximately 100 km north) at Burnt Mountain (SNOTEL site 942) measured seasonal variations of <1 kPa with higher pressures during the summer. The amplitude of the barometric pressure variations is significantly less than that due to snow loading and is likely insufficient to explain the velocities at STD and JUN. Weekly variations in barometric pressure there are on the order of 3–4 kPa, which could contribute to some of the misfit in our inversions, as we do not allow velocities to change on timescales shorter than 2 weeks.

One way to discriminate between possible sources is if we filter the coda in separate frequency bands (1–5 and 5–10 Hz; Figure 9). The higher frequency velocity changes are greater than the lower frequency changes in September, and the reverse is observed in March. If we assume the 1–5 Hz energy is sampling deeper than 5–10 Hz due to the frequency-dependent depth sampling of surface waves in the coda, this result suggests that the peak velocities in September are located shallower than in March, which is most consistent with shallow fluid saturation variations.

6.2. Response to Nisqually Earthquake

Decreases in seismic velocity are commonly observed following earthquakes, particularly on soft soils, and have been interpreted by other authors as nonlinear response to shaking, which heals on the timescale of seconds to years [*Dodge and Beroza*, 1997; *Li et al*., 2007; *Rubenstein et al*., 2007; *Brenguier et al*., 2008b;

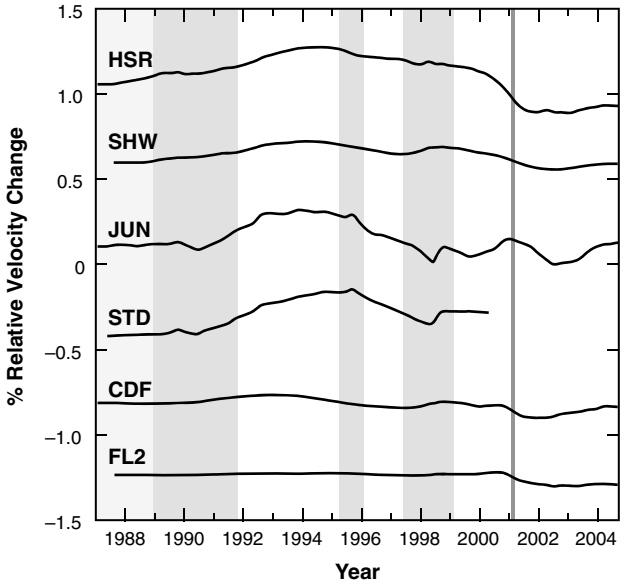

Figure 10. Inversion solution with greater weight of smoothing regularization, mostly damping the annual signal with the exception of 1989 and 1998 on stations JUN and STD due to the large amount of pairs. Vertical line corresponds to time of Nisqually earthquake; the step-like decrease in velocity has also been smoothed as a result of the increased regularization. Times of increased deep seismicity and deformation are highlighted in gray, at the same times as in Figure 1.

Sawazaki et al., 2009; *Wegler et al*., 2009; *Yamada et al*., 2010; *Tatagi et al*., 2012]. One clear nonannual signal is a sharp decrease in velocity in early 2001 of 0.2% at CDF and FL2, 0.5% at SHW, and 0.7% at HSR (it is unresolved at STD due to a low number of pairs crossing the date of the earthquake, and difficult to objectively quantify at JUN). The timing of this decrease corresponds exactly with the 28 February 2001, *M*6.8 Nisqually earthquake, which occurred 113 km to the NNW of MSH at 52 km depth.

The Nisqually earthquake is unique in that it is the only large or local earthquake that coincides with an observable change in velocity in our data. There are no obvious changes during the times of the *M*5.8 Satsop earthquake in 1999, the *M*5.4 Duvall earthquake in 1996, a nearby *M*4.9 in 1989, or the more distant *M*7.9 Denali earthquake in Alaska in 2002. The Nisqually earthquake imparted peak ground acceleration (PGA) on the order of 6 to 7% g to the entire network at MSH, based on the PNSN ShakeMap. This was likely the strongest shaking during the 18 year study period; all other earthquakes cited above had estimated PGA less than 2% g at MSH. However, this acceleration is low compared to the level of shaking considered in the literature, where the largest changes also occur near the rupture. Additionally, the velocity does not recover in at least the next 3 years as one might expect for a nonlinear soil-related response, and there is no appreciable difference between the amplitude in different frequency bands, further suggesting that the velocity change is not concentrated at the surface. Given the distance from the earthquake and that the observed changes are concentrated nearest the volcano's summit, the most likely explanation is a dynamic yet permanent response to shaking. *Battaglia et al*. [2012] studied the response of Yasur volcano to a nearby *M*7.3 earthquake and also found the maximum change that occurred near the summit. PGA and velocity changes at Yasur are comparable, though slightly higher, than MSH for Nisqually (0.5–3.5% velocity change and ~15% g). *Battaglia et al*. [2012] proposed opening of cracks near the volcanic conduit due to permeability enhancement [*Rojstaczer et al*., 1995] or exsolution of magmatic gases as possible explanations for decreased velocity at Yasur, which may also be appropriate to apply at MSH.

6.3. Long-Term Trends

By increasing the weight of the regularization in the inversion, we can damp out the annual signal to more clearly compare long-term trends without introducing unnecessary artifacts from filtering the best fit. One by-product is smoothing of steps in velocity, such as due to the Nisqually earthquake or any smaller steps that might be present but obscured by the large annual signal. Figure 10 shows the result of damping the inversion just enough to eliminate the seasonal signal. The velocities increase and decrease in roughly the same way for most of the stations, though with different amplitudes. This similarity leads us to believe that the signal is real and not a station-specific artifact. Also, it is small or nonexistent on stations far away from the volcano (CDF, FL2) and slightly smaller for stations near the summit (SHW, HSR) than further from the summit (STD, JUN).

We do not see a relationship between the times of deep swarms and the sense of velocity change. Velocities generally increase during the 1989–1992 and 1998 swarms and perhaps decrease around 1995, but such changes are not unique to just these time periods. There is no convincing evidence of magma injection that

Table 2. Parameters for Estimating Surface Strain Due to a Pressure Increase at Depth

ΔP	v	μ	c_1	c_2	α
5 MPa	0.25	1.0e10 Pa	6500 m	11500 m	500 m

would presumably change velocities during the other periods, indicating the majority of the long-term signal is persistent and likely not directly related to magmatic injection. Although we find no conclusive evidence for a change in velocity during the times of proposed intrusions, it is still possible that some changes are volcanic in origin or potentially related to accumulation of exsolved gases from depth. We also note that, as mentioned before, 1996 was a dry year and may be partially to blame for the relative decrease in velocity. If that is the case, an alternative explanation for the long-term trend is that it is related to variability in the water table over the course of several years. Again, without well data we cannot independently verify whether this is the case. Other possibilities for increasing velocity are the growth of Crater Glacier or settling of the dome, but the large signal at more distant stations suggests a distributed source.

7. Discussion

For the 1987–2004 time period at MSH the subsurface velocity structure appears to respond to small stress changes, such as those due to the loads imparted by seasonal precipitation and shaking from a distant large earthquake. However, we do not see any correlations between velocity changes and the time when injections of magma have been proposed to occur beneath MSH. A possible explanation for why we do not see any evidence of magma injection is that velocity changes caused by intrusions were small and/or localized where we have little sensitivity with this method, which is limited to the providing information only about the volume sampled by coda waves. As we have seen from the similarity of velocity changes for shallow and deep earthquakes, coda waves may not sample the deeper part of the magmatic system, where magma likely was accumulating in 1987–2004, as much as the shallower subsurface. Successful detection of deeper changes in velocity associated with small injections of new magma may depend on favorable occurrence of well-distributed deeper earthquakes and dense scattering. However, we expect that a velocity change due to an intrusion would not be limited to the chamber alone and would be distributed around the chamber and to the surface as the host rock deforms due to the increased pressure in the system.

Let us consider the amplitude of a velocity change at the surface due to increased pressure in the magma chamber. We know from *Moran* [1994] that focal mechanisms of deep earthquakes corresponded to pressure changes within an approximately cylindrical magma chamber, which increased from below lithostatic pressure during 1980 to above lithostatic pressure in 1987–1992. Although there is a large trade-off between parameters, especially chamber radius and pressure, misfits decreased significantly for pressures more than 5 MPa above lithostatic pressure. We solve for near-surface deformation and strain for this pressure increase within the magma chamber by approximating it as an oblate spheroid following *Bonaccorso and Davis* [1999] and *Lisowski* [2006]

$$u_r = \frac{\alpha^2 \Delta P}{4\mu r}\left(\frac{c_1^3}{R_1^2} + \frac{2c_1(-3+5v)}{R_1} + \frac{5c_2^3(1-2v) - 2c_2 r^2(-3+5v)}{R_2^3}\right) \tag{3}$$

$$u_t = 0 \tag{4}$$

$$u_z = \frac{\alpha^2 \Delta P}{4\mu r}\left(\frac{c_1^2}{R_1^2} + \frac{2(-2+5v)}{R_1} + \frac{c_2^3(3-10v) - 2r^2(-3+5v)}{R_2^3}\right) \tag{5}$$

$$\varepsilon_{rr} = \frac{\partial u_r}{\partial_r} \tag{6}$$

$$\varepsilon_{tt} = \frac{u_r}{r} \tag{7}$$

$$\varepsilon_{zz} = \frac{v}{1-v}(\varepsilon_{rr} + \varepsilon_{tt}) \tag{8}$$

where u is displacement in the radial, tangential, and up directions; ε is strain; ΔP is change in pressure; α is the radius of the chamber; c_1 is the depth of the top of the chamber; c_2 is the depth to the bottom of the chamber; r is horizontal distance from the center of the chamber; $R_1 = \sqrt{r^2 + c_1^2}$ and $R_1 = \sqrt{r^2 + c_2^2}$ are the

Table 3. Parameters for Estimating Murnaghan Constant *m*

	v	*E*	ϕ	*p*	d*v*/*v*	*m*/μ
Snow load	0.25	1.0e10 Pa	1[a]	10 to 20 kPa	+0.7%	−6e3 to −1e4
Water table			0.2	10 to 90 kPa	+1.0%	−9e3 to −8e4

[a]Assumes water exists only as snow above the surface.

distances from a point on the surface to the top and bottom of the chamber, respectively; ν is Poisson's ratio; and μ is the elastic modulus. For Mount St. Helens we assume values listed in Table 2.

Strain can then be related to change in shear velocity by using a simplified form of *Hughes and Kelly* [1953, equation (11)]

$$\frac{dv_{12}}{v_{12}} = \frac{2m\theta + n\varepsilon_{33}}{4\mu} \tag{9}$$

where *m* and *n* are two of the three Murnaghan third-order elastic constants, μ is the shear modulus, θ is dilatation or volumetric strain, and ε_{33} is strain perpendicular to the direction of travel and polarization of the wave (e.g., ε_{zz} for vertically polarized shear wave (SV) velocity). The Murnaghan constants, *m*, *n*, and *l*, account for nonlinear elastic deformation, including opening and closing of cracks. We can estimate the Murnaghan constants using equations proposed in *Tsai* [2011], which relate strain from hydrologic loading to change in velocity. We can combine equations (10) and (17) of *Tsai* [2011] to estimate the magnitude of m/μ at the surface as follows:

$$\frac{m}{\mu} \sim \frac{dv}{v}\left(\frac{E}{(1+\nu)(1-2\nu)\phi p}\right) \tag{10}$$

where μ is the shear modulus, ν is Poisson's ratio, *E* is Young's modulus, ϕ is porosity, *p* is pressure from the height of a column of water (or snow water equivalent), and d*v*/*v* is change in velocity. Using the values in Table 3 under the assumption that the spring velocity changes are a response to direct loading due to the weight of snowpack and the possibility that autumn changes are due to groundwater level, the ratio m/μ is close to -1×10^4, at the high end of observed values in laboratory experiments for highly cracked samples [*Tsai*, 2011]. Without further constraint on the value of *n*, we assume it is close to *m*. Therefore, the

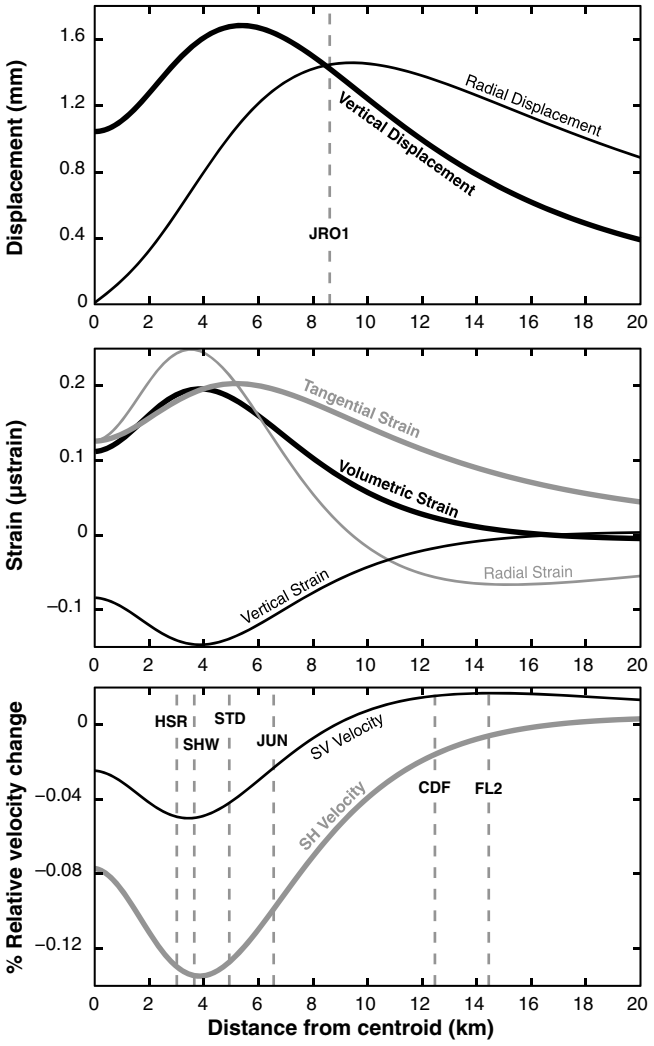

Figure 11. (top) Estimations of displacement, (middle) strain, and (bottom) velocity change at the surface assuming a 5 MPa increase in pressure within the MSH magma chamber. Distances to GPS and seismic stations are noted by vertical lines and labeled. The displacements are at or below the level of detection for GPS motion, consistent with the lack of observed motion. Although SH velocity is above the noise level for velocity change, coda waves are likely much more sensitive to SV velocity, which is below the noise level.

maximum value of change in SV velocity for our theoretical magmatic intrusion is approximately −0.05% (Figure 11). Although strain and velocity increase with depth, this change is still near or below the level of noise with our method, so it is possible that a 5 MPa pressure increase could have escaped detection even without consideration of finite compressibility of a zone around the chamber [*Mastin et al*., 2008; *Dzurisin et al*., 2008]. *Ueno et al*. [2012] observed decreases in velocity of 0.2–0.8% during several intrusion-related swarms with estimated volumes on the order of a few thousand cubic meter; however, these intrusions were also accompanied by measurable surface deformation and volumetric strain of more than 10^{-6}. Our predicted strain is roughly an order of magnitude less than this, consistent with our lack of observable velocity change. The choice of pressure increase is somewhat arbitrary but allows us to estimate an upper bound on the change in pressure in the chamber given our lack of detection to as much as 10 MPa for a chamber of 500 m radius.

8. Conclusions

We used CWI to create a continuous record of seismic velocity change using triggered earthquake data spanning nearly two decades to investigate the history of magma injection and pressurization of the MSH magmatic system. This method is complementary to other studies of velocity change using continuous data, such as ambient noise interferometry, but can be applied to older data sets where continuous data are unavailable and only a triggered record exists. Temporal resolution of velocity change is dependent on the rate of repeating seismicity and could also be applied to more frequent swarms of earthquakes, like those during volcanic eruptions, to produce a record of velocity change on a significantly shorter timescale than presented here.

In this study, we did not resolve a velocity change due to magmatic intrusion(s), though the lack of velocity change directly attributable to the volcano between the 1980–1986 and 2004–2008 eruptions is consistent with a lack of precursory deformation. We concede that it is possible that intrusions occurred but did not pressurize the chamber enough to alter the shallow velocity structure to which this technique is most sensitive. We estimate the maximum pressure change that could have escaped our detection to be on the order of 10 MPa, which is within the previously estimated bounds of pressure changes determined by deep earthquake focal mechanisms. We found well-resolved seismic velocity changes that are dominated by seasonal variability, likely caused by climatic forcing such as snow loading and shallow water table fluctuations. In addition, the increased rate of seismicity is anticorrelated with the higher velocities in late winter, and we believe this is most likely due to snow unloading. The most significant nonseasonal signal is a decrease in velocity at the time of the Nisqually earthquake, during which shaking dynamically likely caused a permanent alteration of the velocity structure. We suggest that the shallow seismicity and observed velocity changes are indications that the volcano was pressurized and sensitive to relatively small pressure changes of a few kilopascals well before the 2004 eruption.

Acknowledgments

Waveform data and earthquake catalog used in this paper are courtesy of the Pacific Northwest Seismic Network and are freely available upon request. The authors would like to thank Seth Moran, Weston Thelen, Stephanie Prejean, Steve Malone, and Matt Haney for discussions during preparation of the text and Weston Thelen and Florent Brenguier for their reviews.

References

Battaglia, J., J. -P. Métaxian, and E. Garaebiti (2012), Earthquake-volcano interaction imaged by coda wave interferometry, *Geophys. Res. Lett.*, *39*, L11309, doi:10.1029/2012GL052003.

Bedrosian, P. A., M. Burgess, and A. Hotovec (2008), Groundwater hydrology within the crater of Mount St. Helens from geophysical constraints, *Eos Trans. AGU*, *89*(53), 2847 Fall Meet. Suppl., Abstract V43E-2191.

Ben-Zion, Y., and P. Leary (1986), Thermoelastic strain in a half-space covered by unconsolidated material, *Bull. Seismol. Soc. Am.*, *76*, 1447–1460.

Bonaccorso, A., and P. M. Davis (1999), Models of ground deformation from vertical volcanic conduits with application to eruptions of Mount St. Helens and Mount Etna, *J. Geophys. Res.*, *104*(B5), 10,531–10,542.

Brenguier, F., N. M. Shapiro, M. Campillo, V. Ferrazzini, Z. Duputel, O. Coutant, and A. Nercessian (2008a), Towards forecasting volcanic eruptions using seismic noise, *Nat. Geosci.*, *1*, 126–130, doi:10.1038/ngeo104.

Brenguier, F., M. Campillo, C. Hadziioannou, N. M. Shapiro, R. M. Nadeau, and E. Larose (2008b), Postseismic relaxation along the San Andreas Fault at Parkfield from continuous seismological observations, *Science*, *321*, 1478–1481, doi:10.1126/science.1160943.

Carmona, E., J. Almendros, J. A. Peña, and J. M. Ibáñez (2010), Characterization of fracture systems using precise array locations of earthquake multiplets: An example at Deception Island volcano, Antarctica, *J. Geophys. Res.*, *115*, B06309, doi:10.1029/2009JB006865.

Christiansen, L. B., S. Hurwitz, M. O. Saar, S. E. Ingebritsen, and P. A. Hsieh (2005), Seasonal seismicity at western United States volcanic centers, *Earth Planet. Sci. Lett.*, *240*, 307–321.

Dodge, D. A., and G. C. Beroza (1997), Source array analysis of coda waves near the 1989 Loma Prieta, California, mainshock: Implications for the mechanism of coseismic velocity changes, *J. Geophys. Res.*, *102*(B11), 24,437–24,458.

Dzurisin, D., M. Lisowski, M. P. Poland, D. R. Sherrod, and R. G. LaHusen (2008), Constraints and conundrums resulting from ground-deformation measurements made during the 2004-2005 dome-building eruption of Mount St. Helens, Washington, in *A Volcano*

Rekindled: The Renewed Eruption of Mount St. Helens, 2004–2006, edited by D. R. Sherrod, W. E. Scott, and P. H. Stauffer, *Prof. Paper 1750*, chap. 14, pp. 281–300, U.S. Geol. Surv., Reston, Va.

Gerlach, T. M., K. A. McGee, and M. P. Doukas (2008), Emission rates of CO_2, SO_2, and H_2S, scrubbing, and preeruption excess volatiles at Mount St. Helens, 2004–2005, in *A Volcano Rekindled: The Renewed Eruption of Mount St. Helens, 2004–2006*, edited by D. R. Sherrod, W. E. Scott, and P. H. Stauffer, *Prof. Paper 1750*, chap. 26, pp. 543–571, U.S. Geol. Surv., Reston, Va.

Grêt, A., R. Snieder, and J. Scales (2006), Time-lapse monitoring of rock properties with coda wave interferometry, *J. Geophys. Res.*, *111*, B03305, doi:10.1029/2004JB003354.

Hughes, D. S., and J. L. Kelly (1953), Second-order elastic deformation of solids, *Phys. Rev.*, *92*, 1145–1149.

Hurwitz, S., K. L. Kipp, S. E. Ingebritsen, and M. E. Reid (2003), Groundwater flow, heat transport, and water table position within volcanic edifices: Implications for volcanic processes in the Cascade Range, *J. Geophys. Res.*, *108*(B12), 2557, doi:10.1029/2003JB002565.

Kanu, C. O., R. Snieder, and D. O'Connell (2013), Estimation of velocity change using repeating earthquakes with different locations and focal mechanisms, *J. Geophys. Res. Solid Earth*, *118*, 1–10, doi:10.1002/jgrb.50206.

Lehto, H. L., D. C. Roman, and S. C. Moran (2013), Source mechanisms of persistent shallow earthquakes during eruptive and non-eruptive periods between 1981 and 2011 at Mount St. Helens, Washington, *J. Volcanol. Geotherm. Res.*, *256*, 1–15, doi:10.1016/j.volgeores.2013.02.005.

Li, Y.-G., P. Chen, E. S. Cochran, and J. E. Vidale (2007), Seismic velocity variations on the San Andreas fault caused by the 2004 *M*6 Parkfield Earthquake and their implications, *Earth Planets Space*, *59*, 21–31.

Lisowski, M. (2006) Analytical volcano deformation source models, in *Volcano Deformation: Geodetic Monitoring Techniques*, edited by D. Dzurisin, chap. 8, pp. 279–304, Springer-Praxis, Chichester, U. K.

Lisowski, M., D. Dzurisin, R. P. Denlinger, and E. Y. Iwatsubo (2008), Analysis of GPS-measured deformation associated with the 2004–2006 dome-building eruption of Mount St. Helens, Washington, in *A Volcano Rekindled: The Renewed Eruption of Mount St. Helens, 2004–2006*, edited by D. R. Sherrod, W. E. Scott, and P. H. Stauffer, *Prof. Paper 1750*, chap. 15, pp. 301–333, U.S. Geol. Surv., Reston, Va.

Massin, F., J. Farrell, and R. B. Smith (2013), Repeating earthquakes in the Yellowstone volcanic field: Implications for rupture dynamics, ground deformation, and migration in earthquake swarms, *J. Volcanol. Geotherm. Res.*, *257*, 159–173, doi:10.1016/j.jvolgeores.2013.03.22.

Mastin, L. G. (1994), Explosive tephra emissions at Mount St. Helens, 1989–1991: The violent escape of magmatic gas following storms?, *Geol. Soc. Am. Bull.*, *106*(2), 175–185.

Mastin, L. G., E. Roeloffs, N. M. Beeler, and J. E. Quick (2008), Constraints on the size, overpressure, and oolatile content of the Mount St. Helens magma system from geodetic and dome-growth measurements during the 2004–2006+ eruption, in *A Volcano Rekindled: The Renewed Eruption of Mount St. Helens, 2004–2006*, edited by D. R. Sherrod, W. E. Scott, and P. H. Stauffer, *Prof. Paper 1750*, chap. 22, pp. 461–488, U.S. Geol. Surv., Reston, Va.

Meier, U., N. M. Shapiro, and F. Brenguier (2010), Detecting seasonal variations in seismic velocities within Los Angeles basin from correlations of ambient seismic noise, *Geophys. J. Int.*, *181*, 985–996.

Moran, S. C. (1994), Seismicity at Mount St. Helens, 1987–1992: Evidence for repressurization of an active magmatic system, *J. Geophys. Res.*, *99*(B3), 4341–4354.

Moran, S. C., S. D. Malone, A. I. Qamar, W. A. Thelen, A. K. Wright, and J. Caplan-Auerbach (2008), Seismicity associated with renewed dome building at Mount St. Helens, 2004–2005, in *A Volcano Rekindled: The Renewed Eruption of Mount St. Helens, 2004–2006*, edited by D. R. Sherrod, W. E. Scott, and P. H. Stauffer, *Prof. Paper 1750*, chap. 2, pp. 27–60, U.S. Geol. Surv., Reston, Va.

Musumeci, C., S. Gresta, and S. D. Malone (2002), Magma system recharge of Mount St. Helens from precise relative hypocenter location of microearthquakes, *J. Geophys. Res.*, *107*(B10), 2264, doi:10.1029/2001JB000629.

Nakamura, A., A. Hasegawa, N. Hirata, T. Iwasaki, and H. Hamaguchi (2002), Temporal variations of seismic wave velocity associated with 1998 M6.1 Shizukuishi earthquake, *Pure Appl. Geophys.*, *159*, 1183–1204.

Pacheco, C., and R. Snieder (2005), Time-lapse travel time change of multiply scattered acoustic waves, *J. Acoust. Soc. Am.*, *118*(3), 1300–1310.

Pallister, J. S., C. R. Thornber, K. V. Cashman, M. A. Clynne, H. A. Lowers, C. W. Mandeville, I. K. Brownfield, and G. P. Meeker (2008), Petrology of the 2004–2006 Mount St. Helens lava dome—Implications for magmatic plumbing and eruption triggering, in *A Volcano Rekindled: The Renewed Eruption of Mount St. Helens, 2004–2006*, edited by D. R. Sherrod, W. E. Scott, and P. H. Stauffer, *Prof. Paper 1750*, chap. 30, pp. 648–702, U.S. Geol. Surv., Reston, Va.

Pandolfi, D., C. J. Bean, and G. Saccorotti (2006), Coda wave interferometric detection of seismic velocity changes associated with the 1999 M = 3.6 event at Mt. Vesuvius, *Geophys. Res. Lett.*, *33*, L06306, doi:10.1029/2005GL025355.

Petersen, T. (2007), Swarms of repeating long-period earthquakes at Shishaldin Volcano, Alaska, 2001–2004, *J. Volcanol. Geotherm. Res.*, *166*, 177–192, doi:10.1016/j.jvolgeores.2007.07.014.

Poland, M. P., and Z. Lu (2008), Radar interferometry observations of surface displacements during pre- and coeruptive periods at Mount St. Helens, Washington, 1992–2005, in *A Volcano Rekindled: The Renewed Eruption of Mount St. Helens, 2004–2006*, edited by D. R. Sherrod, W. E. Scott, and P. H. Stauffer, *Prof. Paper 1750*, chap. 18, pp. 361–382, U.S. Geol. Surv., Reston, Va.

Poupinet, G., W. L. Ellsworth, and J. Frechet (1984), Monitoring velocity variations in the crust using earthquake doublets: An application to the Calaveras Fault, California, *J. Geophys. Res.*, *89*(B7), 5719–5731.

Ratdomopurbo, A., and G. Poupinet (1995), Monitoring a temporal change of seismic velocity in a volcano: Application to the 1992 eruption of Mt. Merapi (Indonesia), *Geophys. Res. Lett.*, *22*(7), 775–778.

Rojstaczer, S., S. Wolf, and R. Michel (1995), Permeability enhancement in the shallow crust as a cause of earthquake-induced hydrological changes, *Nature*, *373*, 237–239.

Rubenstein, J. L., N. Uchida, and G. C. Beroza (2007), Seismic velocity reductions caused by the 2003 Tokachi-Oki earthquake, *J. Geophys. Res.*, *112*, B05315, doi:10.1029/2006JB004440.

Saccorotti, G., I. Lokmer, C. J. Bean, G. Di Grazia, and D. Patanè (2007), Analysis of sustained long-period activity at Etna Volcano, Italy, *J. Volcanol. Geotherm. Res.*, *160*, 340–354, doi:10.1016/.jvolgeores.2006.10.008.

Sawazaki, K., H. Sato, H. Nakahara, and T. Nishimura (2009), Time-lapse changes of seismic velocity in the shallow ground caused by strong ground motion shock of the 2000 Western-Tottori earthquake, Japan, as revealed from coda deconvolution analysis, *Bull. Seismol. Soc. Am.*, *99*(1), 352–366, doi:10.1785/0120080058.

Scott, W. E., D. R. Sherrod, and C. A. Gardner (2008), Overview of the 2004 to 2006, and continuing, eruption of Mount St. Helens, Washington, in *A Volcano Rekindled: The Renewed Eruption of Mount St. Helens, 2004–2006*, edited by D. R. Sherrod, W. E. Scott, and P. H. Stauffer, *Prof. Paper 1750*, chap. 1, pp. 3–22, U.S. Geol. Surv., Reston, Va.

Sens-Schönfelder, C., and U. Wegler (2006), Passive image interferometry and seasonal variations of seismic velocities at Merapi Volcano, Indonesia, *Geophys. Res. Lett.*, *33*, L21302, doi:10.1029/2006GL027797.

Silver, P. G., T. M. Daley, F. Niu, and E. L. Majer (2007), Active source monitoring of cross-well seismic travel time for stress-induced changes, *Bull. Seismol. Soc. Am.*, *97*(1B), 281–293, doi:10.1785/0120060120.

Snieder, R. (2002), Coda wave interferometry and the equilibration of energy in elastic media, *Phys. Rev. E*, *66*, 046615, doi:10.1103/PhysRevE.66.046615.

Snieder, R. (2006), The theory of coda wave interferometry, *Pure Appl. Geophys.*, *163*, 455–473, doi:10.1007/s00024-005-0026-6.

Snieder, R., A. Grêt, H. Douma, and J. Scales (2002), Coda wave interferometry for estimating nonlinear behavior in seismic velocity, *Science*, *295*, 2253–2255.

Tatagi, R., T. Okada, H. Nakahara, N. Umino, and A. Hasegawa (2012), Coseismic velocity change in and around the focal region of the 2008 Iwate-Miyagi Nairiku earthquake, *J. Geophys. Res.*, *117*, B06315, doi:10.1029/2012JB009252.

Thelen, W. A., R. S. Crosson, and K. C. Creager (2008), Absolute and relative locations of earthquakes at Mount St. Helens, Washington, using continuous data: Implications for magmatic processes, in *A Volcano Rekindled: The Renewed Eruption of Mount St. Helens, 2004–2006*, edited by D. R. Sherrod, W. E. Scott, and P. H. Stauffer, *Prof. Paper 1750*, chap. 4, pp. 71–95, U.S. Geol. Surv., Reston, Va.

Thelen, W., S. Malone, and M. West (2011), Multiplets: Their behavior and utility at dacitic and andesitic volcanic centers, *J. Geophys. Res.*, *116*, B08210, doi:10.1029/2010JB007924.

Tsai, V. C. (2011), A model for seasonal changes in GPS positions and seismic wave speeds due to thermoelastic and hydrologic variations, *J. Geophys. Res.*, *116*, B04404, doi:10.1029/2010JB008156.

Ueno, T., T. Saito, K. Shiomi, B. Enescu, H. Hirose, and K. Obara (2012), Fractional seismic velocity change related to magma intrusions during earthquake swarms in the eastern Izu peninsula, central Japan, *J. Geophys. Res.*, *117*, B12305, doi:10.1029/2012JB009580.

Wegler, U., B.-G. Lühr, R. Snieder, and A. Ratdomopurbo (2006), Increase of shear wave velocity before the 1998 eruption of Merapi volcano (Indonesia), *Geophys. Res. Lett.*, *33*, L09303, doi:10.1029/2006GL025928.

Wegler, U., H. Nakahara, C. Sens-Schönfelder, M. Korn, and K. Shiomi (2009), Sudden drop of seismic velocity after the 2004 M_w 6.6 mid-Niigata earthquake, Japan, observed with Passive Image Interferometry, *J. Geophys. Res.*, *114*, B06305, doi:10.1029/2008JB005869.

Yamada, M., J. Mori, and S. Ohmi (2010), Temporal changes of subsurface velocities during strong shaking as seen from seismic interferometry, *J. Geophys. Res.*, *115*, B03302, doi:10.1029/2009JB006567.